Article

Upconversion and Color Tunability in Er^{3+}–Tm^{3+}–Yb^{3+} Tri-Doped Fluorophosphate Glasses

Fernando Rivera-López [1,*] , **Palamandala Babu** [2] , **Vemula Venkatramu** [3] **and Víctor Lavín** [4]

1 Departamento de Ingeniería Industrial, Escuela Superior de Ingeniería y Tecnología, Universidad de La Laguna, Apdo. 456, E-38200 San Cristóbal de La Laguna, Santa Cruz de Tenerife, Spain
2 Department of Physics, NTR Government Degree College, Vayalpad 517 299, India
3 Department of Physics, Yogi Vemana University, Kadapa 516 005, India
4 Departamento de Física, IUdEA, and MALTA Consolider Team, Universidad de La Laguna, Apdo. 456, E-38200 San Cristóbal de La Laguna, Santa Cruz de Tenerife, Spain
* Correspondence: frivera@ull.es

Abstract

A series of Er^{3+}–Tm^{3+}–Yb^{3+} tri-doped fluorophosphate glasses with different molar compositions were synthesized using the conventional melt-quenching technique, and their optical properties were measured and analyzed. Under laser excitation at 980 nm, blue, green and red upconverted emissions were observed at around 475, 545 and 660 nm, respectively. Based on the results and the energy level diagrams, energy transfer processes were proposed to explain the population mechanisms of the emitting levels. A final characterization was developed within the framework of the CIE 1931 chromaticity coordinate diagram. Varying the doping concentrations of the optically active rare-earth ions, as well as the laser pumping power, enabled modulation of the three primary colors, resulting in blue, green and relatively close to white light emissions. This tunability of the upconverted emissions highlights the potential of these fluorophosphate glasses as tunable optical devices, laser systems and visual show effects.

Keywords: luminescence; upconversion; color display; fluorophosphate glass; Er^{3+}; Tm^{3+}; Yb^{3+}

1. Introduction

During the last few years, the study of materials doped with optically active trivalent rare-earth (RE^{3+}) ions has attracted much interest due to their potential in photonic applications, such as solid-state lasers [1,2], color displays [3–5] or optical amplifiers [6]. One of the features of RE^{3+} ions is their ability to convert near-infrared (NIR) energy into visible light, a process known as upconversion [7–12]. Among all RE^{3+} dopants, trivalent Erbium (Er^{3+}) is a very interesting ion that can be excited with commercial low-cost diode lasers at around 800, 860 and 980 nm. Its intermediate low-energy metastable levels, with long lifetimes, allow green and red upconverted emissions to be obtained at around 550 and 650 nm, respectively. Another interesting ion is trivalent Thulium (Tm^{3+}), with a very intense blue emission at around 475 nm. For both optically active ions, upconverted emissions can be enhanced by the addition of the trivalent Ytterbium (Yb^{3+}) ion, which acts as an efficient sensitizer for the upconversion mechanisms [13]. Regarding the state of the art, it is worth highlighting the studies on Er^{3+}–Tm^{3+}–Yb^{3+} tri-doped samples, such as those performed on oxides [14–18], phosphates [19,20], fluorides [21–23] and fluorophosphates [24]. In these systems, the right combination of blue, green and red emissions, originating from Er^{3+} and

Tm^{3+} ions, can be modulated through the relative concentrations of the ions or the pump power excitation, which is of particular interest for optical technologies.

Fluorophosphate glasses doped with RE^{3+} ions, such as Er^{3+}, Tm^{3+} and Yb^{3+}, offer significant advantages over conventional phosphate or metaphosphate glasses, as well as over oxide and fluoride glasses for optical and photonic applications. First, the fluorophosphate matrix combines the favorable structural and chemical properties of phosphate glasses with the low vibrational energy characteristic of fluoride bonds [25], lower than those of oxides, resulting in reduced absorption losses due to non-radiative relaxation processes. This enables higher light emission efficiency and better protection of the excited states of the dopant ions, which is crucial for the efficiency of processes such as upconversion [24]. In contrast, phosphate and metaphosphate glasses exhibit a higher density of high-energy vibrational states due to P–O–P bonds [1], which decreases the emission efficiency of the RE^{3+} ions. Therefore, fluorophosphate glasses doped with these ions stand out as superior materials for the development of advanced optical devices, such as fiber amplifiers, lasers and white lighting, where material efficiency and stability are paramount. These reasons constitute the rationale for choosing fluorophosphate over other hosts, along with the scarcity of reports on upconversion luminescence color tunability in Er^{3+}, Tm^{3+} and Yb^{3+} tri-doped fluorophosphate glasses.

Among the various possible combinations to obtain a fluorophosphates glass, the following combination was selected for synthesis: P_2O_5, 17 K_2O, (11-x/2-y/2) BaO, 9 Al_2O_3, 6 BaF_2, 2 Yb_2O_3, x Er_2O_3 and y Tm_2O_3. P_2O_5 based glasses have the advantages of high transparency [26], a low melting temperature [21,27] and good thermal stability and chemical durability [28]. Another advantage of phosphate glasses is that they can be easily fabricated into different shapes and sizes. As for the possible components, the incorporation of potassium oxide (K_2O) reduces the melting temperature, barium oxide (BaO) enhances the mechanical properties, which is very important for fiber production [29], and the addition of aluminum trioxide (Al_2O_3) increases chemical stability [30]. However, a disadvantage when phosphate glasses are employed as a laser host is that they have large thermal expansion and their phonon energies are relatively high. The addition of barium fluoride (BaF_2) leads to a decrease in the OH^- free group [31], thus reducing the phonon energy and, consequently, the non-radiative de-excitation processes involving optically active ions.

In this work, fluorophosphate glasses with a fixed Yb_2O_3 concentration and different concentrations of Er_2O_3 and Tm_2O_3 were synthesized. The upconverted luminescence of these glasses were studied in detail under 980 nm laser excitation. According to the Commission Internationale de I'Eclairage (CIE) 1931 chromaticity diagram, the upconverted emissions were characterized in order to study the potential interest of this fluorophosphate glass for photonic applications.

2. Materials and Methods

Glasses with chemical compositions (in mol%) of (55-x/2-y/2) P_2O_5, 17 K_2O, (11-x/2-y/2) BaO, 9 Al_2O_3, 6 BaF_2, 2 Yb_2O_3, x Er_2O_3 and y Tm_2O_3 (where x and y ranges from 0.01 to 1) were prepared by the well-known melt-quenching technique at room temperature. The precursor oxides and fluoride were well grounded in an agate mortar with a pestle. The batch composition taken in a platinum crucible was placed in a furnace and melted at a temperature range of 1323–1373 K (1050–1100 °C) for 1 h, poured onto a preheated brass plate and finally annealed at 623 K (350 °C) for 10 h in order to remove the thermal strains. The samples were then carefully polished with silicon carbide abrasive paper and a polishing film for optical measurements. All samples showed a very homogeneous structure and transparency. The composition and labels of the samples are given in Table 1.

Table 1. Composition and labels of the fluorophosphate glasses.

Glass Composition (mol%)	Label
54.99 P_2O_5 -17 K_2O -10.99 BaO- 9 Al_2O_3 -6 BaF_2 -2 Yb_2O_3 -0.01 Er_2O_3 -0.01 Tm_2O_3	PF001Er001Tm
54.90 P_2O_5 -17 K_2O -10.90 BaO -9 Al_2O_3 -6 BaF_2 -2 Yb_2O_3 -0.1 Er_2O_3 -0.1 Tm_2O_3	PF01Er01Tm
54.00 P_2O_5 -17 K_2O -10.00 BaO -9 Al_2O_3 -6 BaF_2 -2 Yb_2O_3 -1 Er_2O_3 -1 Tm_2O_3	PF1Er1Tm
54.50 P_2O_5 -17 K_2O -10.50 BaO -9 Al_2O_3 -6 BaF_2 -2 Yb_2O_3 -0.5 Er_2O_3 -0.5 Tm_2O_3	PF05Er05Tm
54.45 P_2O_5 -17 K_2O -10.45 BaO -9 Al_2O_3 -6 BaF_2 -2 Yb_2O_3 -0.1 Er_2O_3 -1 Tm_2O_3	PF01Er1Tm
54.70 P_2O_5 -17 K_2O -10.70 BaO -9 Al_2O_3 -6 BaF_2 -2 Yb_2O_3 -0.1 Er_2O_3 -0.5 Tm_2O_3	PF01Er05Tm
54.45 P_2O_5 -17 K_2O -10.45 BaO -9 Al_2O_3 -6 BaF_2 -2 Yb_2O_3 -1 Er_2O_3 -0.1 Tm_2O_3	PF1Er01Tm
54.70 P_2O_5 -17 K_2O -10.70 BaO -9 Al_2O_3 -6 BaF_2 -2 Yb_2O_3 -0.5 Er_2O_3 -0.1 Tm_2O_3	PF05Er01Tm

X-ray Diffraction (XRD) analyses were carried out in a PANalytical Empyrean diffractometer using a Cu anode $Cu_{K\alpha1,2}$ radiation ($\lambda_{K\alpha1}$ = 1.5406 Å and $\lambda_{K\alpha2}$ = 1.5444 Å). The measurements were recorded at 0.02626° intervals throughout the 5–80 2θ range. To acquire Scanning Electron Microscopy (SEM) and Energy-Dispersive X-ray Spectroscopy (EDS) images, a ZEISS EVO 15 electron microscope, with an acceleration of 15 kV, was used. The sample surface was coated with a thin layer of carbon.

Absorption spectra were measured using a spectrophotometer (Cary5000). Upconverted luminescence spectra were measured by excitation with a commercial continuous-wave (cw) diode laser at 980 nm (CNI Laser, model MDL-III-80-2W). The RE^{3+} ion emissions were focused onto a 0.18 m focal length single-grating monochromator (Jobin Yvon Triax 180), with a resolution of 0.5 nm, and were then detected with a photomultiplier tube (Hamamatsu R-928). All measurements were made at room temperature and were corrected for the spectral response of the equipment.

3. Results and Discussion

XRD analyses were performed to investigate the internal structure. As can be observed in Figure 1, the resulting diffractogram exhibits a broad halo centered at around 27 2θ (°), which is characteristic of an amorphous structure. Non-crystalline materials display diffuse X-ray scattering due to their disordered structure and the absence of long-range translational symmetry. The absence of sharp Bragg peaks confirms the lack of a long-range atomic order, supporting the vitreous nature of these fluorophosphate samples.

Complementary to XRD, a morphological analysis was carried out using SEM and EDS mapping. As can be seen in Figure 2, SEM and EDS images reveal a homogeneous and uniform morphology, with no evidence of phase separation, porosity, clusters or crystallite formation. Furthermore, elemental mapping confirms an even distribution of the constituent elements across the samples, consistent with a well-mixed glassy matrix. These results further support the structural uniformity and amorphous nature of the glass. The homogeneous dispersion of RE^{3+} ions in the glass matrix prevents concentration quenching and promotes efficient energy transfer processes. Moreover, this finding is particularly significant, as it allows the excitation of the samples regardless of the specific region being excited, ensuring that the luminescence response remains independent of the excitation area.

The intraconfigurational transitions observed in the absorption spectrum of the fluorophosphate glass doped with 2 mol% of Yb_2O_3, 1 mol% of Er_2O_3 and 1 mol% of Tm_2O_3 (PF1Er1Tm sample) are presented in Figure 3. The transitions start from the $^4I_{15/2}$ ground state to the multiplets of the Er^{3+} ion (labeled in green), and from the $^3H_6$ ground state to the multiplets of the Tm^{3+} ion (labeled in blue). In addition, the only intraconfigurational *f-f* absorption band for the Yb^{3+} ion is the $^2F_{7/2} \rightarrow {}^2F_{5/2}$ transition at the beginning of the NIR range, with a maximum at 975 nm (labeled in red).
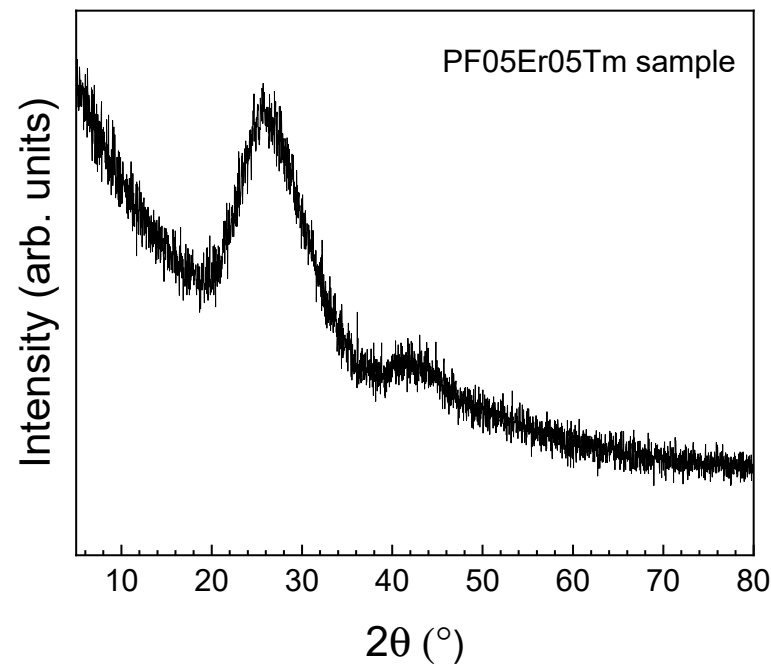
Figure 1. XRD of the fluorophosphate glass doped with 2 mol% of Yb_2O_3, 0.5 mol% of Er_2O_3 and 0.5 mol% of Tm_2O_3.
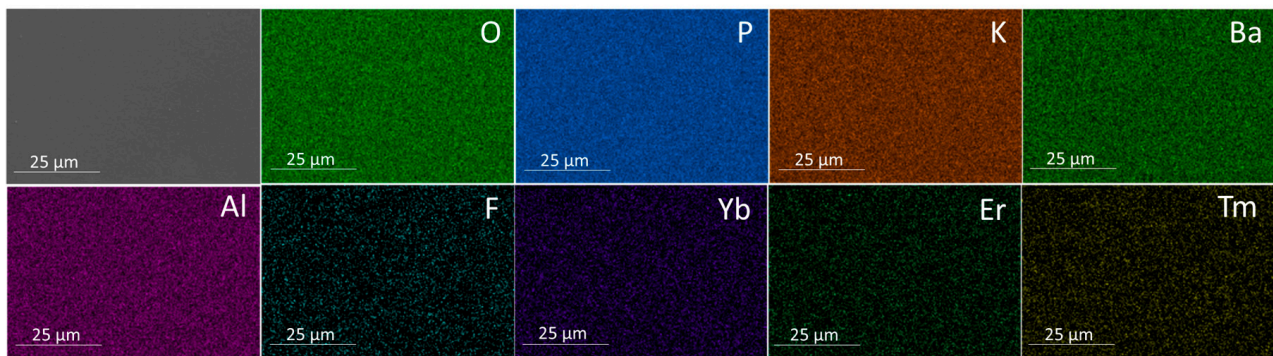

Figure 2. SEM and EDS images of the fluorophosphate glass doped with 2 mol% of Yb_2O_3, 0.5 mol% of Er_2O_3 and 0.5 mol% of Tm_2O_3.

The upconverted luminescence spectra from 300 to 700 nm were obtained after exciting the tri-doped samples with a cw 980 nm diode laser, in resonance with the $^2F_{7/2} \rightarrow {}^2F_{5/2}$ absorption transition of the Yb^{3+} ions and the $^4I_{15/2} \rightarrow {}^4I_{11/2}$ transition of the Er^{3+} ions. The obtained results for all the samples are shown in Figure 4, in which three clear upconverted emission bands in the blue, green and red ranges are observed. The blue band, centered at around 475 nm, can be attributed to the $^1G_4 \rightarrow {}^3H_6$ transition of the Tm^{3+} ions, whereas the green emission is composed of two thermalized bands of Er^{3+}, related to the hypersensitive $^2H_{11/2} \rightarrow {}^4I_{15/2}$ transition at 525 nm and the $^4S_{3/2} \rightarrow {}^4I_{15/2}$ transition at 545 nm. Finally, the red emission, centered at 660 nm, is associated with the $^4F_{9/2} \rightarrow {}^4I_{15/2}$ transition of the Er^{3+} ions. All relevant electronic *f-f* transitions of these RE^{3+} ions and their partial energy level diagrams are shown in Figure 5. As can be seen in Figure 4, when the Er^{3+} concentration increases, green and red emissions also increase, whereas the blue emission is favored when the Tm^{3+} ion concentration increases. In the case of the PF1Er01Tm sample, a green emission in the vicinity of white light was observed by the naked eye.
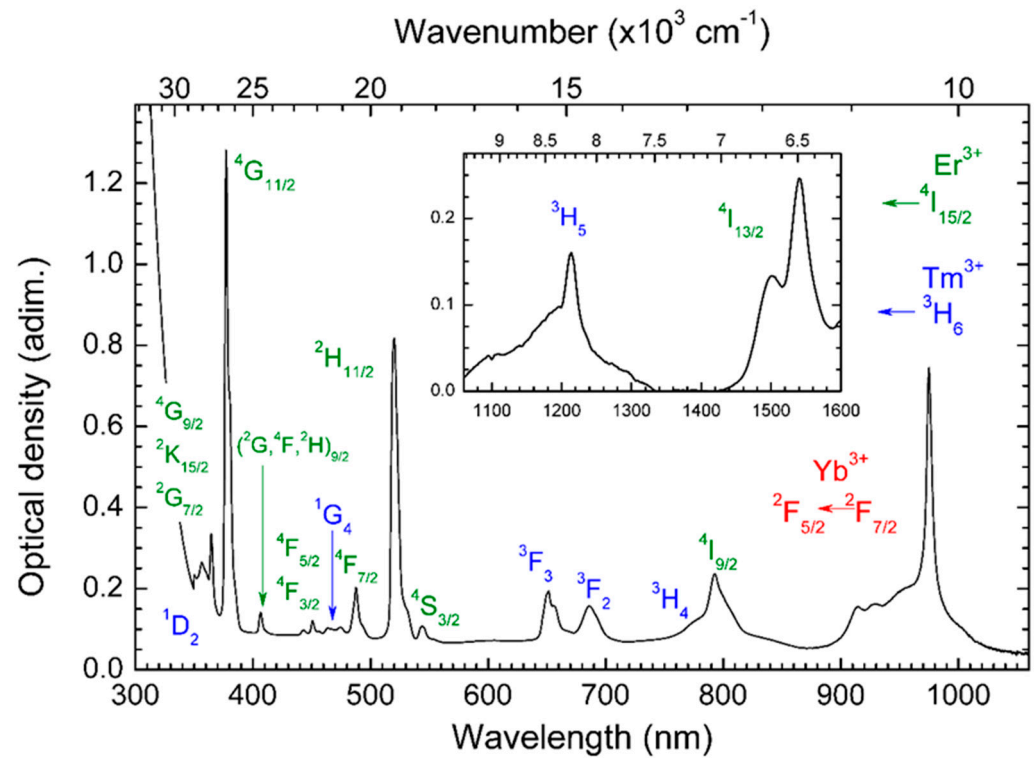
Figure 3. Absorption spectrum of the fluorophosphate glass doped with 2 mol% of Yb_2O_3, 1 mol% of Er_2O_3 and 1 mol% of Tm_2O_3. The transitions start from the $^4I_{15/2}$ ground state to the multiplets of the Er^{3+} ion (labeled in green), and from the $^3H_6$ ground state to the multiplets of the Tm^{3+} ion (labeled in blue). The only intraconfigurational *f-f* absorption band for the Yb^{3+} ion is the $^2F_{7/2} \rightarrow {}^2F_{5/2}$ transition (labeled in red).
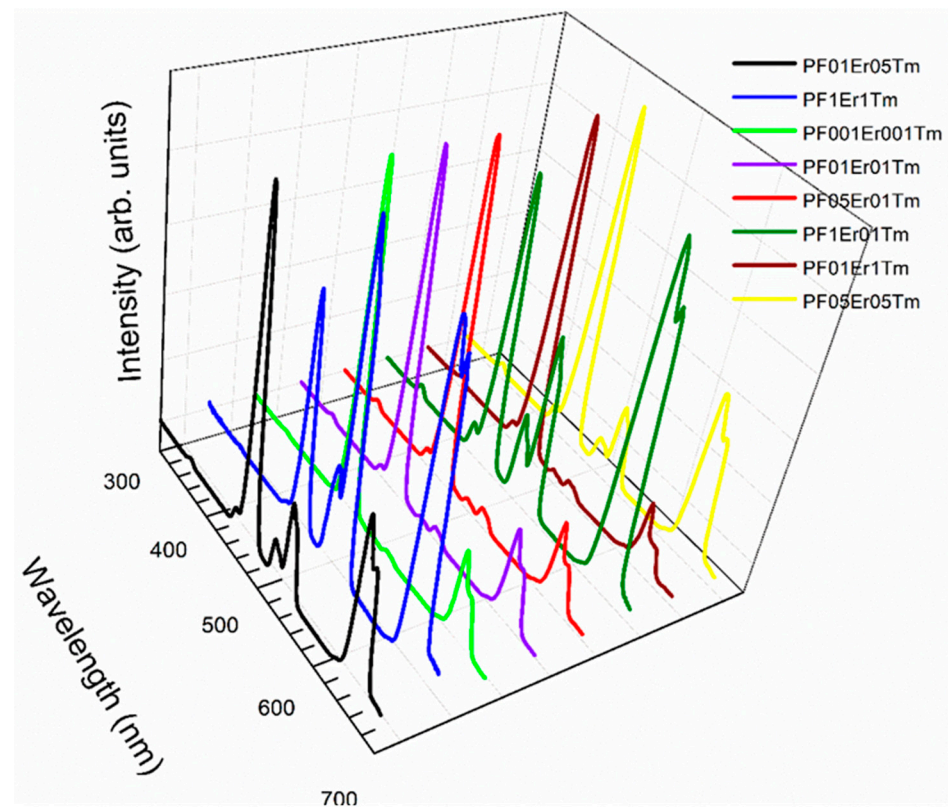
Figure 4. Upconverted emission spectra of Er^{3+}–Tm^{3+}–Yb^{3+} tri-doped fluorophosphate glasses under cw laser excitation at 980 nm.
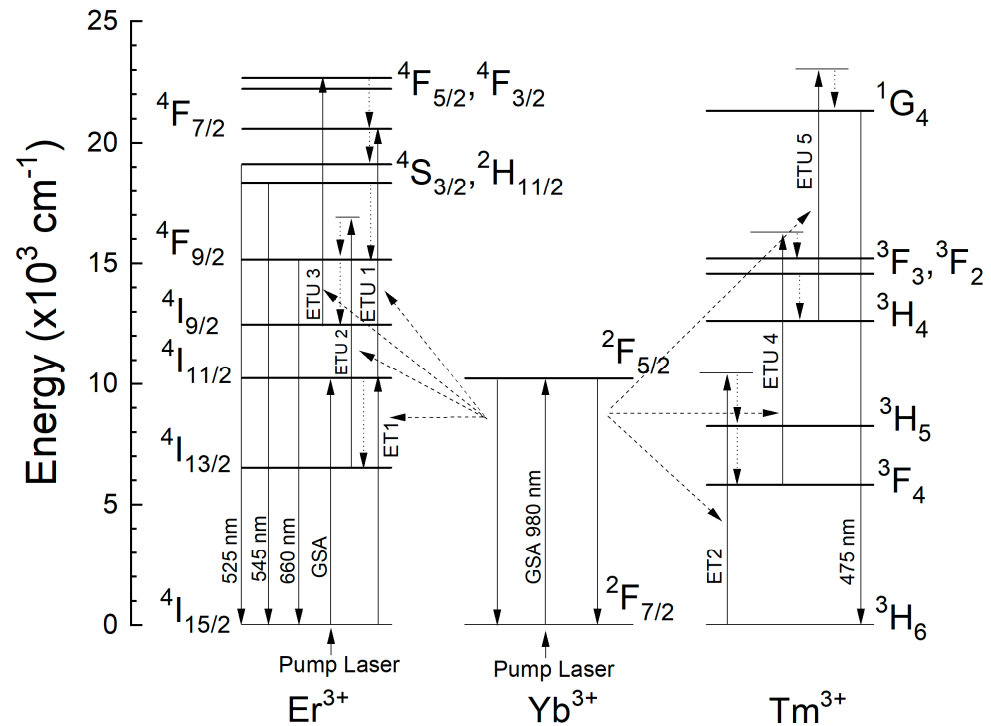
Figure 5. Partial energy level diagrams of the Er^{3+}, Tm^{3+} and Yb^{3+} ions showing the possible energy transfer upconversion mechanisms after cw laser excitation at 980 nm. Labels of the observed upconverted emission bands are also shown.

With the aim of investigating the mechanisms involved in the population of the emitting levels, the upconverted emission intensities were measured as a function of the laser pumping power. The emission intensity, I_{em}, is proportional to the n-th power of the incident laser pump power, P_{pump}, according to the following expression [32]:

$$I_{em} = \left(P_{pump}\right)^{n} \tag{1}$$

where n represents the number of photons absorbed per upconverted photon emitted. Figure 6 shows a double logarithmic plot of the integrated emission intensities of the blue, green and red upconverted emissions as a function of the incident laser pump power.

Linear least squares fitting of the experimental results to Equation (1) were calculated up to 100 mW. Powers higher than 100 mW were not considered because saturation occurs, and the proportionality of Equation (1) is valid only for unsaturated upconverted emissions. Based on these fits, slopes of 2.8, 2.3 and 1.9 were obtained for the blue, green and red upconverted emissions, respectively, indicating that three photons are required for blue emission, whereas two photons are required for red emission [33]. The slope of 2.3 for the green emission could be attributed to the involvement of three photons, which is different from the usual two photons reported by other authors, such as Pavitra et al., Shi et al. and Chen et al. [34–36], but is consistent with the findings reported by Bai et al., Li et al. and Hassairi et al. [37–39].

The change in slopes may be attributed to the saturation of the excited states of the Er^{3+} and Tm^{3+} ions, resulting from efficient energy transfer from the Yb^{3+} ions. Furthermore, as shown in Figure 6, saturation occurs at approximately the same excitation power for all three emissions, suggesting that it could be associated with the saturation of Yb^{3+} ion absorption. These phenomena result in a decrease in energy transfer upconversion (ETU) luminescence. Moreover, the increase in laser power raises the temperature, which may promote non-radiative processes, resulting in a loss of useful energy and contributing

to saturation. It should be noted that in our experiments, the samples were subjected to continuous laser excitation of up to 300 mW over an extended period of 1 h. During this time, we carefully monitored the samples and their emission intensities, and no photobleaching or degradation was observed. The emissions remained stable throughout the irradiation period, indicating that these glasses maintain their luminescent properties under conditions relevant to their practical use.
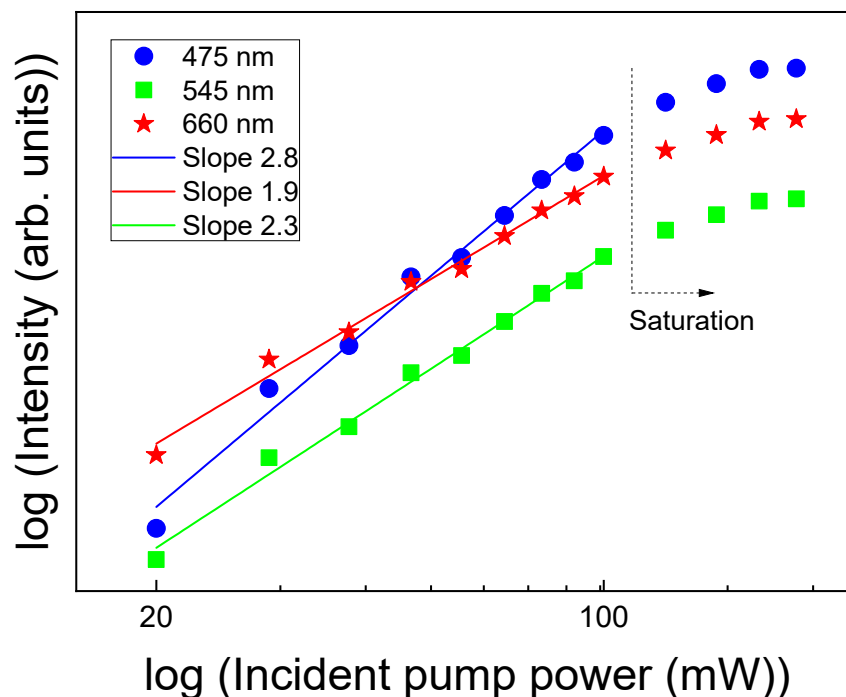

Figure 6. Double logarithmic plot of the integrated emission intensities of the red (stars), green (squares) and blue (circles) upconverted emissions as a function of the incident laser pumping power at 980 nm.

According to these results, a possible population scheme was proposed in the simplified energy level diagram in Figure 5. First, the green and red upconverted emissions from the Er^{3+} ions were analyzed. Since the absorption cross-section of the Yb^{3+} ion at 980 nm is larger than that of the Er^{3+} ion, together with the fact that the concentration of Yb^{3+} ions is significantly higher, the Er^{3+} ions can be considered to be initially populated by energy transfer from neighboring Yb^{3+} ions, rather than through a ground state absorption (GSA) process. This first energy transfer process, denoted as ET1, involves a cross-relaxation mechanism with a Yb^{3+} ion at the excited $^2F_{5/2}$ level and an Er^{3+} ion at the $^4I_{15/2}$ ground state. The Yb^{3+} ion de-excitates to the ground state, transferring the transition energy to the Er^{3+} ion, which reaches the $^4I_{11/2}$ metastable level according to the $(^2F_{5/2},^4I_{15/2}) \rightarrow (^2F_{7/2},^4I_{11/2})$ scheme. In the following steps, the thermally coupled green emitting $(^2H_{11/2},^4S_{3/2})$ levels can be populated via ETU and excited state absorption (ESA). For the samples co-doped with Yb^{3+} ions, ETU mechanisms can be considered predominant with respect to ESA [40]. For a two photon process, ETU1 is considered, where the $^4F_{7/2}$ state of the Er^{3+} ions is populated after an energy transfer form Yb^{3+} ions, following the $(^2F_{5/2},^4I_{11/2}) \rightarrow (^2F_{7/2},^4F_{7/2})$ cross-relaxation scheme. Subsequent non-radiative relaxation from the $^4F_{7/2}$ level feeds the $^4S_{3/2}$, $^2H_{11/2}$ and $^4F_{9/2}$ emitting levels. However, a three photon process must be taken into account based on the dependence of the green emission on the laser pumping power. In this case, after populating the $^4I_{11/2}$ level, via ET1, a non-radiative relaxation feeds the $^4I_{13/2}$ level. From this state, the ETU2 process takes place following the $(^2F_{5/2},^4I_{13/2}) \rightarrow (^2F_{7/2},^4F_{9/2})$ cross-relaxation scheme, from which non-

radiative de-excitation populates the $^4I_{9/2}$ level. The third photon is absorbed from the $^4I_{9/2}$ level, where the ETU3 process takes place, feeding the $^4F_{5/2}$ level according to the $(^2F_{5/2},^4I_{9/2})\rightarrow(^2F_{7/2},^4F_{5/2})$ scheme. Finally, the subsequent non-radiative de-excitations populate the thermally-coupled green-emitting $(^2H_{11/2},^4S_{3/2})$ levels.

For the blue emission, the population of Tm^{3+} ions occurs via energy transfer because there are no Stark levels in resonance with the laser excitation at 980 nm. The process for populating the $^1G_4$ emitting level can be described as a phonon-assisted energy transfer mechanism involving three laser photons. After cw laser excitation at 980 nm, the Yb^{3+} ions are promoted to the $^2F_{5/2}$ level, from which a non-resonant energy transfer to a neighboring Tm^{3+} ion, denoted as ET2, populates the $^3H_5$ level following the $(^2F_{5/2},^3H_6)\rightarrow(^2F_{7/2},^3H_5)$ scheme. From the $^3H_5$ level, non-radiative relaxation feeds the lower $^3F_4$ level, and then a second non-resonant energy transfer, labeled as ETU4, takes place according to the $(^2F_{5/2},^3F_4)\rightarrow(^2F_{7/2},^3F_3)$ cross-relaxation scheme. Subsequent multi-phonon de-excitation from the $^3F_3$ and $^3F_2$ levels populates the $^3H_4$ level, from which a third non-resonant energy transfer, labeled as ETU5 and associated with the $(^2F_{5/2},^3H_4)\rightarrow(^2F_{7/2},^1G_4)$ mechanism, populates the $^1G_4$ level from which blue emission is produced after radiative de-excitation to the ground state.

It is worth noting that increasing concentrations of Tm^{3+} and Er^{3+} ions also lead to an increase in the energy transfer probabilities from the emitting levels, which means a decrease in the efficiency of the upconverted emissions. There are several cross-relaxation energy transfer channels between Tm^{3+} ions involving the blue emitting level, as well as between Er^{3+} ions involving the green and red emitting levels, which are fully described in the literature [41,42]. In addition, there are inter-ion resonant, or quasi-resonant, cross-relaxation channel energy transfer mechanisms between the different doped ions that also contribute to increases in this non-radiative de-excitation, such as:

Tm^{3+}-Er^{3+} CR1: $(^1G_4,^4I_{15/2})\rightarrow(^3H_6,^4F_{7/2})$
Tm^{3+}-Er^{3+} CR2: $(^1G_4,^4I_{15/2})\rightarrow(^3F_4,^4F_{9/2})$
Tm^{3+}-Er^{3+} CR3: $(^1G_4,^4I_{15/2})\rightarrow(^3H_5,^4I_{9/2})$
Er^{3+}-Tm^{3+} CR4: $(^4S_{3/2},^3H_6)\rightarrow(^4I_{11/2},^3H_5)$
Er^{3+}-Tm^{3+} CR5: $(^4S_{3/2},^3H_6)\rightarrow(^4I_{9/2},^3F_4)$
Er^{3+}-Tm^{3+} CR6: $(^4F_{9/2},^3H_6)\rightarrow(^4I_{13/2},^3H_5)$
Er^{3+}-Tm^{3+} CR7: $(^4F_{9/2},^3H_6)\rightarrow(^3H_6,^3F_3)$

which force a compromise between the concentration levels and the maximum upconterved emission of photons in the blue, green and red ranges of visible light.

Within the framework of the CIE 1931, the *XY* chromaticity coordinate graph for the study of the color purity of the glass sample emissions was plotted (Figure 7). The CIE 1931 plot comprises a triangle where the position in the diagram is known the chromaticity point. The chromatic coordinates *(x, y)*, presented in Table 2, were evaluated using the following expressions:

$$x = \frac{X}{X+Y+Z} \cdot y = \frac{Y}{X+Y+Z} \cdot z = \frac{Z}{X+Y+Z} \tag{2}$$

$$X = \int I(\lambda)\overline{x}d\lambda \tag{3}$$

$$Y = \int I(\lambda)\overline{y}d\lambda \tag{4}$$

$$Z = \int I(\lambda)\overline{z}d\lambda \tag{5}$$

where *X*, *Y* and *Z* represent the tristimulus values; λ corresponds to the wavelength; $(\overline{x}, \overline{y}, \overline{z})$ are the three color-matching functions; and *I(λ)* represents the emission spectra of the

samples. Table 2 presents the *(x, y)* chromaticity coordinates for the samples under laser excitation at 980 nm and with a laser pumping power of 100 mW.
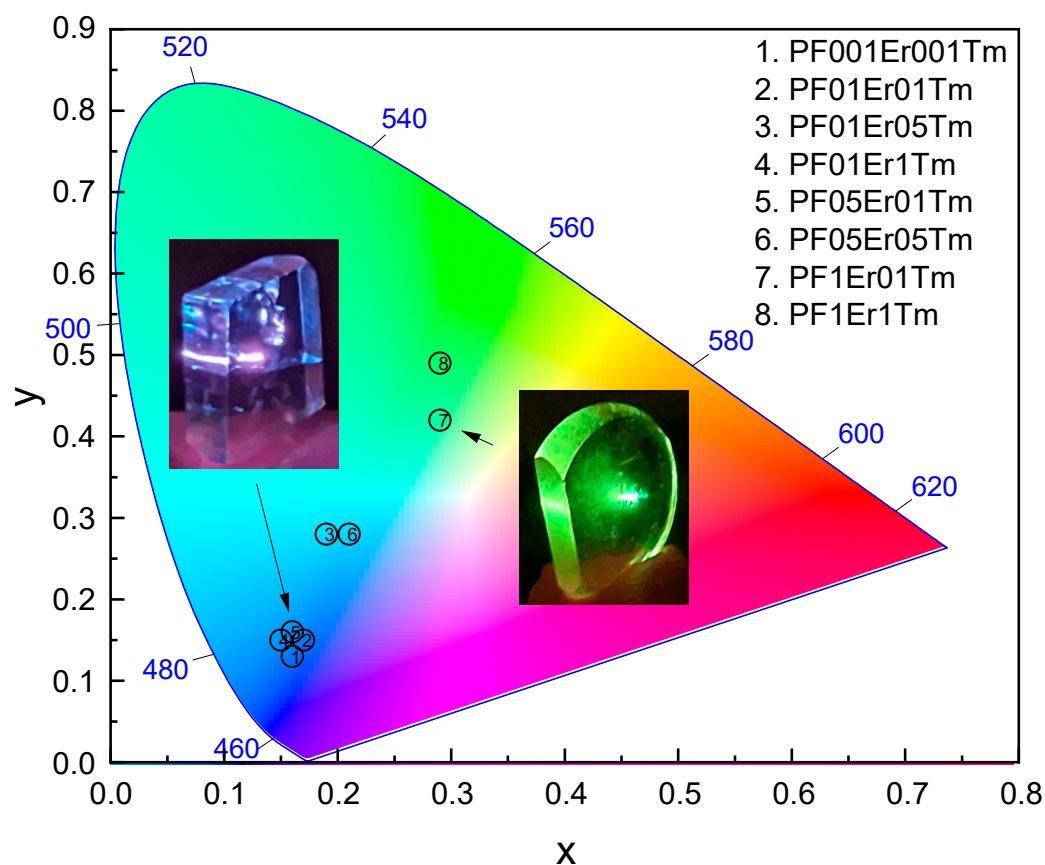

Figure 7. Representation on the CIE 1931 diagram of the chromaticity coordinates associated with the upconverted emissions of fluorophosphate glasses (power = 100 mW). The sample emitting green corresponds to PF1Er01Tm, and the one emitting blue is PF05Er01Tm.

Table 2. Chromaticity coordinates *(x, y)* for all samples under excitation at 980 nm and 100 mW power.

Sample	Chromaticity Coordinates
PF001Er001Tm	$x = 0.16$, $y = 0.13$
PF01Er01Tm	$x = 0.17$, $y = 0.15$
PF1Er1Tm	$x = 0.29$, $y = 0.49$
PF05Er05Tm	$x = 0.21$, $y = 0.28$
PF01Er1Tm	$x = 0.15$, $y = 0.15$
PF01Er05Tm	$x = 0.19$, $y = 0.28$
PF1Er01Tm	$x = 0.29$, $y = 0.42$
PF05Er01Tm	$x = 0.16$, $y = 0.16$

As can be observed in Figure 7, at 100 mW laser power excitation, the PF1Er1Tm and PF1Er01Tm samples fall close to the green region. The samples PF001Er001Tm, PF01Er01Tm, PF01Er1Tm and PF05Er01Tm fall in the blue region, whereas PF05Er05Tm and PF01Er05Tm are relatively close to the white region. This behavior depends on the balance of blue, green and red emissions, which is influenced by the Er^{3+} and Tm^{3+} concentrations.

In order to study the color tunability, the upconverted emissions were recorded under varying levels of laser pumping power. Figure 8 represents the CIE 1931 chromaticity diagram as a function of the laser pumping power for sample PF01Er05Tm. Table 3 shows,

for this sample, the dependence of the chromaticity coordinates *(x, y)* on the excitation power, ranging from 20 to 200 mW.
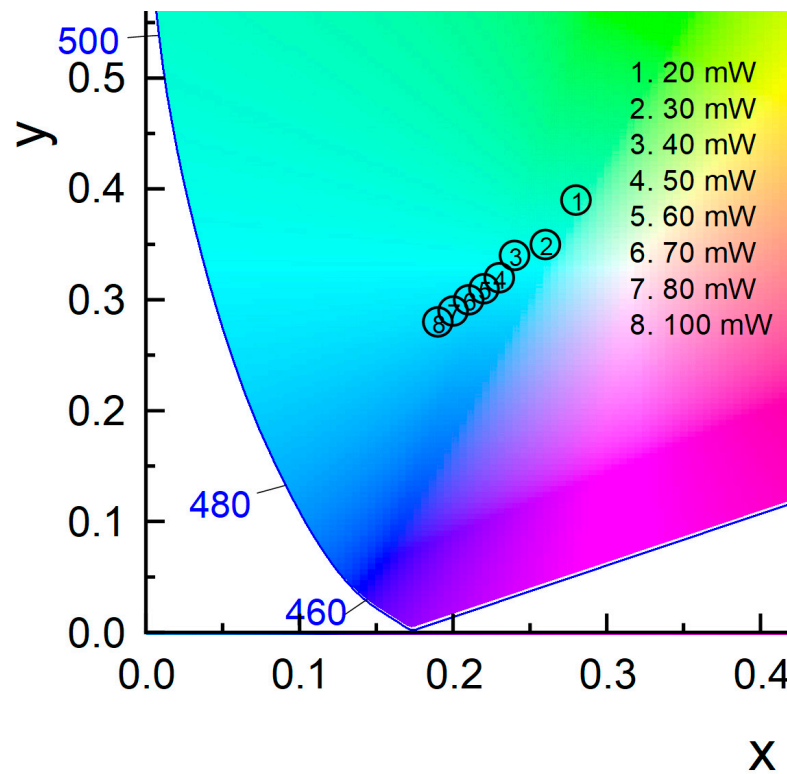

Figure 8. Representation on the CIE 1931 diagram of the chromaticity coordinates associated with the upconverted emissions of sample PF01Er05Tm, varying the laser power from 20 to 100 mW.

Table 3. Dependence of chromaticity coordinates *(x, y)* on excitation power for the PF01Er05Tm sample, varying the laser pump power from 20 to 200 mW.

Power (mW)	Chromaticity Coordinates
20	$x = 0.28, y = 0.39$
30	$x = 0.26, y = 0.35$
40	$x = 0.24, y = 0.34$
50	$x = 0.23, y = 0.32$
60	$x = 0.22, y = 0.31$
70	$x = 0.21, y = 0.30$
80	$x = 0.20, y = 0.29$
90	$x = 0.20, y = 0.29$
100	$x = 0.19, y = 0.28$
125	$x = 0.19, y = 0.27$
150	$x = 0.19, y = 0.27$
175	$x = 0.19, y = 0.27$
200	$x = 0.19, y = 0.27$

From Figure 8, as the pumping power increases, the x and y values decrease, whereas the z value increases. The chromaticity coordinates *(x, y)* change from (0.28, 0.39) at 20 mW to (0.19, 0.28) at 100 mW. At a laser power above 100 mW, no changes are observed as a consequence of the saturation effect. Figure 8 shows that increasing the excitation power shifts the chromaticity coordinates towards the blue region in the color diagram. This is due to the increase in blue emission as the pumping power increases, in good agreement with observations by Pavitra et al. [34] in SrY_2O_4 nanocrystalline phosphors. As can be

seen, the obtained values cover a wide region, indicating that light can be modulated by adjusting the pumping power.

Continuing the comparison with other results reported in the literature, these glasses, with a lower power range than other studies, such as $Ca_9Y(PO_4)_7$ phosphor [19], cover a wider region of the chromaticity diagram than $NaNbO_3$ nanocrystals [16] and SrY_2O_4 nanocrystalline phosphors [34]. By varying the concentrations of optically active ions, broad emission tuning is achieved, spanning from the green to the blue region. This range is comparable to that reported by Liang et al. for fluorosilicate glasses [43], with the difference that their samples exhibited emissions from the blue region up to the upper blue region. The results obtained in our study are comparable to those reported in the literature. Although we were unable to generate pure white light from our samples, improved color tunability was achieved by varying both the concentration of the active ions and the excitation pump power.

4. Conclusions

Er^{3+}–Tm^{3+}–Yb^{3+} tri-doped phosphate glasses, with different RE^{3+} concentrations, were synthesized using a conventional melt-quenching technique. Under cw laser excitation at 980 nm, intense blue, green and red upconverted emissions were observed. The intensities of these emissions depend on the concentrations of the optically active ions. For these samples, the combination of primary colors produced blue and green light, and in some cases, light in the vicinity of white, as observed in the CIE 1931 chromaticity diagram. In addition, varying the laser pumping power enables modulation of the light. In view of these results, Er^{3+}–Tm^{3+}–Yb^{3+} tri-doped fluorophosphate glasses can be considered materials with great potential for application in various optical technologies, such as color displays, upconversion lasers, tunable lasers and show effects.

References

1. Rivera-López, F.; Babu, P.; Basavapoornima, C.; Jayasankar, C.K.; Lavín, V. Efficient $Nd^{3+} \rightarrow Yb^{3+}$ energy transfer processes in high phonon energy phosphate glasses for 1.0 μm Yb^{3+} laser. *J. Appl. Phys.* **2011**, *109*, 123514. [CrossRef]

2. Rivera-López, F.; Lavín, V. Upconversion/back-transfer losses and emission dynamics in Nd^{3+}-Yb^{3+} co-doped phosphate glasses for multiple pump channel laser. *J. Non-Cryst. Solids* **2018**, *489*, 84–90. [CrossRef]

3. Pattnaik, S.; Mondal, M.; Mukhopadhyay, L.; Rai, V.K. Trivalent lanthanide doped orthovanadate phosphors for efficient upconversion. *Mater. Today Proc.* **2019**, *46*, 6363–6366. [CrossRef]

4. Wu, X.; Zhao, X.; Ren, Q.; Du, L.; Pei, M.; Hai, O. Triple luminescent center energy transfer enables color tuning in Na_3Y. *Polyhedron* **2022**, *225*, 116047. [CrossRef]

5. Babu, P.; Jang, K.H.; Kim, E.S.; Shi, L.; Seo, H.J.; Rivera-López, F.; Rodríguez-Mendoza, U.R.; Lavín, V.; Vijaya, R.; Jayasankar, C.K.; et al. Spectral investigations on Dy^{3+}-doped transparent oxyfluoride glasses and nanocrystalline glass ceramics. *J. Appl. Phys.* **2009**, *105*, 013516. [CrossRef]

6. Rivera-López, F.; Babu, P.; Jyothi, L.; Rodríguez-Mendoza, U.R.; Martín, I.R.; Jayasankar, C.K.; Lavín, V. Er^{3+}–Yb^{3+} codoped phosphate glasses used for an efficient 1.5μm broadband gain medium. *Opt. Mater.* **2012**, *34*, 1235–1240. [CrossRef]

7. Auzel, F. Upconversion and Anti-Stokes Processes with f and d Ions in Solids. *Chem. Rev.* **2004**, *104*, 139–173. [CrossRef] [PubMed]

8. Rivera-López, F.; Torres, M.E.; de Cos, G.G. Upconversion and cooperative luminescence in YBO_3:Yb^{3+}–Er^{3+}. *Mater. Today Commun.* **2021**, *27*, 102434. [CrossRef]

9. Gaponenko, N.V.; Staskov, N.I.; Sudnik, L.V.; Vityaz, P.A.; Luchanok, A.R.; Karnilava, Y.D.; Lashkovskaya, E.I.; Stepikhova, M.V.; Yablonskiy, A.N.; Zhivulko, V.D.; et al. Upconversion Luminescence from Sol-Gel-Derived Erbium- and Ytterbium-Doped $BaTiO_3$ Film Structures and the Target Form. *Photonics* **2023**, *10*, 359. [CrossRef]

10. Pominova, D.; Proydakova, V.; Romanishkin, I.; Kuznetsov, S.; Linkov, K.; Tabachkova, N.; Ryabova, A. $NaGdF_4$:Yb, Tm Upconversion Nanoparticles for Bioimaging in Shortwave-Infrared Range: Study of Energy Transfer Processes and Composition Optimization. *Photonics* **2024**, *11*, 38. [CrossRef]

11. Sola, D.; Miguel, A.; Arias-Egido, E.; Peña, J.I. Spectroscopy and near-infrared to visible upconversion of Er^{3+} ions in aluminosilicate glasses manufactured with controlled optical transmission. *Appl. Sci.* **2021**, *11*, 1137. [CrossRef]

12. Zi, Y.; Huang, A.; Zhao, H.; Bai, X.; Xu, Z.; Ullah, A.; Liu, Y.; Cun, Y.; Song, Z.; Qiu, J.; et al. Efficient Reversible Upconversion Luminescence Modulation based on Photochromism of Lanthanides-Doped $BaMgSiO_4$ Glass Ceramics Toward Optical Storage Application. *Laser Photonics Rev.* **2024**, *18*, 2400882. [CrossRef]

13. Patra, A.; Friend, C.S.; Kapoor, R.; Prasad, P.N. Upconversion in Er^{3+}:ZrO_2 Nanocrystals. *J. Phys. Chem. B* **2002**, *106*, 1909–1912. [CrossRef]

14. Yang, J.; Zhang, C.; Peng, C.; Li, C.; Wang, L.; Chai, R.; Lin, J. Controllable Red, Green, Green, Blue (RGB) and bright white upconversion luminescence of Lu_2O_3:Yb^{3+}/Er^{3+}/Tm^{3+} nanocrystals through single laser excitation at 980 nm. *Chem. A Eur. J.* **2009**, *15*, 4649–4655. [CrossRef] [PubMed]

15. Zheng, K.; Zhang, D.; Zhao, D.; Liu, N.; Shi, F.; Qin, W. Bright white upconversion emission from Yb^{3+}, Er^{3+}, and Tm^{3+}-codoped Gd_2O_3 nanotubes. *Phys. Chem. Chem. Phys.* **2010**, *12*, 7620–7625. [CrossRef] [PubMed]

16. Kumar, U.U.; Vijaya, N.; Oliva, J.; Jacinto, C.; de La Rosa, E.; Jayasankar, C.K. Multicolor upconversion emission and color tunability in Tm^{3+}/Er^{3+}/Yb^{3+} Tri-Doped $NaNbO_3$ nanocrystals. *Mater. Express* **2012**, *2*, 294–302. [CrossRef]

17. Yan, D.; Zhu, J.; Wu, H.; Yang, Z.; Qiu, J.; Song, Z.; Yu, X.; Yang, Y.; Zhou, D.; Yin, Z.; et al. Energy transfer and photoluminescence modification in Yb-Er-Tm triply doped $Y_2Ti_2O_7$ upconversion inverse opal. *J. Mater. Chem.* **2012**, *22*, 18558–18563. [CrossRef]

18. Carmo, F.F.D.; Nascimento, J.P.C.D.; Façanha, M.X.; Sales, T.O.; Santos, W.Q.; Gouveia-Neto, A.S.; Jacinto, C.; Sombra, A.S.B. White light upconversion emission and color tunability in Er^{3+}/Tm^{3+}/Yb^{3+} tri-doped $YNbO_4$ phosphor. *J. Lumin.* **2018**, *204*, 676–684. [CrossRef]

19. Du, S.; Wang, D.; Wang, Y.; Xin, S.; Qiang, Q.; Ma, X. Synthesis and up-conversion luminescence of Yb^{3+}/Er^{3+}/Tm^{3+} doped $Ca_9Y(PO_4)_7$. *New J. Chem.* **2015**, *39*, 5605–5611. [CrossRef]

20. Hassairi, M.A.; Hernández, A.G.; Dammak, M.; Zambon, D.; Chadeyron, G.; Mahiou, R. Tuning white upconversion emission in $GdPO_4$:Er/Yb/Tm phosphors. *J. Lumin.* **2018**, *203*, 707–713. [CrossRef]

21. Li, X.; Xiao, Z.; Luo, M.; Dong, X.; Du, T.; Wang, Y. Low melting glasses in ZnO-Fe_2O_3-P_2O_5 system with high chemical durability and thermal stability for sealing or waste immobilization. *J. Non-Cryst. Solids* **2017**, *469*, 62–69. [CrossRef]

22. Zhu, S.; Xie, X.; Han, L.; Li, H.; Shi, C.; Yang, Y.; Sun, J. Co-doped $NaYF_4$:Yb/Er/Tm upconversion luminescent coating to enhance the efficiency of photovoltaic cells. *Phys. Chem. Chem. Phys.* **2024**, *26*, 17882–17891. [CrossRef] [PubMed]

23. Li, J.; Wang, Y.; Zhang, X.; Li, L.; Hao, H. Up-converting luminescence and temperature sensing of Er^{3+}/Tm^{3+}/Yb^{3+} co-doped $NaYF_4$ phosphors operating in visible and the first biological window range. *Nanomaterials* **2021**, *11*, 2660. [CrossRef] [PubMed]

24. Liao, M.; Hu, L.; Fang, Y.; Zhang, J.; Sun, H.; Xu, S.; Zhang, L. Upconversion properties of Er^{3+}, Yb^{3+} and Tm^{3+} codoped fluorophosphate glasses. *Spectrochim. Acta–Part A Mol. Biomol. Spectrosc.* **2007**, *68*, 531–535. [CrossRef] [PubMed]

25. Cao, X.; Wang, P.; Wan, R.; Guo, C.; Tian, S. Structural insight of fluorophosphate glasses through F/O ratio: Case study of Raman and NMR spectra. *J. Non-Cryst. Solids* **2024**, *637*, 123065. [CrossRef]

26. Kaewjaeng, S.; Chanthima, N.; Thongdang, J.; Reungsri, S.; Kothan, S.; Kaewkhao, J. Synthesis and radiation properties of Li_2O-BaO-Bi_2O_3-P_2O_5 glasses. *Mater. Today Proc.* **2018**, *43*, 2544–2553. [CrossRef]

27. Liu, W.; Pan, Y.T.; Zhang, J.; Zhang, L.; Moya, J.S.; Cabal, B.; Wang, D.Y. Low-melting phosphate glasses as flame-retardant synergists to epoxy: Barrier effects vs flame retardancy. *Polym. Degrad. Stab.* **2021**, *185*, 109495. [CrossRef]

28. Shi, X.Z.; Gu, Y.; Liu, T.Y.; Jiang, Z.H.; Li, R.; Zeng, F. Effect of different P_2O_5/SnF_2 ratios on the structure and properties of phosphate glass. *J. Non-Cryst. Solids* **2022**, *578*, 121350. [CrossRef]

29. Kityk, I.V.; Wasylak, J.; Kucharski, J.; Dorosz, D. PbO-Bi_2O_3-Ga_2O_3 -BaO-Dy^{3+} glasses for IR luminescence. *J. Non-Cryst. Solids* **2002**, *297*, 285–289. [CrossRef]

30. Obaton, A.F.; Labbé, C.; Le Boulanger, P.; Elouadi, B.; Boulon, G. Excited state absorption in Yb^{3+} -Er^{3+} -codoped phosphate glasses (ZnO-Al_2O_3-La_2O_3-P_2O_5) around the $^4I_{13/2} \rightarrow ^4I_{15/2}$ emission spectral range. *Spectrochim. Acta Part A Mol. Biomol. Spectrosc.* **1999**, *55*, 263–271. [CrossRef]

31. Lesniak, M.; Mach, G.; Starzyk, B.; Baranowska, A.; Bik, M.; Kochanowicz, M.; Zmojda, J.; Miluski, P.; Sitarz, M.; Dorosz, D. Investigation of the structure in oxyfluoride TeO_2–P_2O_5 based glasses with the various BaF_2 content. *J. Mol. Struct.* **2020**, *1217*, 128452. [CrossRef]

32. Pollnau, M.; Gamelin, D.; Lüthi, S.; Güdel, H.; Hehlen, M. Power dependence of upconversion luminescence in lanthanide and transition-metal-ion systems. *Phys. Rev. B Condens. Matter Mater. Phys.* **2000**, *61*, 3337–3346. [CrossRef]

33. Jacinto, C.; Vermelho, M.V.D.; Gouveia, E.A.; De Araujo, M.T.; Udo, P.T.; Astrath, N.G.C.; Baesso, M.L. Pump-power-controlled luminescence switching in Yb^{3+} Tm^{3+} codoped water-free low silica calcium aluminosilicate glasses. *Appl. Phys. Lett.* **2007**, *91*, 2007–2009. [CrossRef]

34. Pavitra, E.; Raju, G.S.R.; Oh, J.H.; Yu, J.S. Pump power induced tunable upconversion emissions from $Er^{3+}/Tm^{3+}/Yb^{3+}$ ions tri-doped SrY_2O_4 nanocrystalline phosphors. *New J. Chem.* **2014**, *38*, 3413–3420. [CrossRef]

35. Shi, L.; Li, C.; Shen, Q.; Qiu, Z. White upconversion emission in $Er^{3+}/Yb^{3+}/Tm^{3+}$ codoped $LiTaO_3$ polycrystals. *J. Alloys Compd.* **2014**, *591*, 105–109. [CrossRef]

36. Chen, X.; Zhang, B.; Qian, X.; Wang, J.; Zheng, L.; Hou, J.; Fang, Y.; Su, L. Upconversion color tunability and white light generation in $Yb^{3+}/Er^{3+}/Tm^{3+}$ tri-doped CaF_2 single crystals. *Opt. Mater.* **2019**, *90*, 40–45. [CrossRef]

37. Bai, Y.; Wang, Y.; Peng, G.; Zhang, W.; Wang, Y.; Yang, K.; Zhang, X.; Song, Y. Enhanced white light emission in Er/Tm/Yb/Li codoped Y_2O_3 nanocrystals. *Opt. Commun.* **2009**, *282*, 1922–1924. [CrossRef]

38. Li, Y.; Zhang, J.; Luo, Y.; Zhang, X.; Hao, Z.; Wang, X. Color control and white light generation of upconversion luminescence by operating dopant concentrations and pump densities in Yb^{3+}, Er^{3+} and Tm^{3+} tri-doped Lu_2O_3 nanocrystals. *J. Mater. Chem.* **2011**, *21*, 2895–2900. [CrossRef]

39. Hassairi, M.A.; Dammak, M.; Zambon, D.; Chadeyron, G.; Mahiou, R. Red–green–blue upconversion luminescence and energy transfer in $Yb^{3+}/Er^{3+}/Tm^{3+}$ doped YP_5O_{14} ultraphosphates. *J. Lumin.* **2017**, *181*, 393–399. [CrossRef]

40. Li, Y.; Zhang, Y.; Hong, G.; Yu, Y. Upconversion luminescence of Y_2O_3:Er^{3+}, Yb^{3+} nanoparticles prepared by a homogeneous precipitation method. *J. Rare Earths* **2008**, *26*, 450–454. [CrossRef]

41. Zhang, Y.; Xu, S.; Li, X.; Sun, J.; Zhang, J.; Zheng, H.; Zhong, H.; Hua, R.; Xia, H.; Chen, B. Concentration quenching of blue upconversion luminescence in Tm^{3+}/Yb^{3+} co-doped $Gd_2(WO_4)_3$ phosphors under 980 and 808 nm excitation. *J. Alloys Compd.* **2017**, *709*, 147–157. [CrossRef]

42. Venkatramu, V.; León-Luis, S.F.; Rodríguez-Mendoza, U.R.; Monteseguro, V.; Manjón, F.J.; Lozano-Gorrín, A.D.; Valiente, R.; Navarro-Urrios, D.; Jayasankar, C.K.; Muñoz, A.; et al. Synthesis, structure and luminescence of Er^{3+}-doped $Y_3Ga_5O_{12}$ nano-garnets. *J. Mater. Chem.* **2012**, *22*, 13788–13799. [CrossRef]

43. Liang, H.; Lei, W.; Liu, S.; Zhang, P.; Luo, Z.; Lu, A. Color tunable up-conversion luminescence characteristics of Yb^{3+}-Er^{3+}-Tm^{3+} tri-doped fluorosilicate glass potentially used in WLED field. *Opt. Mater.* **2021**, *119*, 111320. [CrossRef]